Evaluation of Sources of Artificial Light at Night With an Autonomous Payload in a Sounding Balloon Flight

Carlo Bettanini, Mirco Bartolomei, Pietro Fiorentin, Alessio Aboudan, and Stefano Cavazzani

***Abstract*—The presence of artificial light at night is not only limiting astronomical observations but has been linked to negative effects on human health and behavior of wildlife. New measurement systems are therefore needed to monitor artificial light emissions and their time evolution; Misurazione dell' INquinamento LUminoso autonomous payload has been designed and tested at University of Padova to provide complete aerial observations of artificial light sources over extended areas, with the capability to be integrated either on stratospheric balloons or drones. The implemented architecture is based on commercial components and is controlled by a Raspberry PI single board computer with the capability of uninterrupted operation up to 5 h. The payload was successfully launched with a stratospheric sounding balloon on July 8, 2021 from Lajatico (Tuscany) and performed continuous analysis of emission sources up to the burst altitude of 34 km. The article will describe the calibration activity of the imaging unit which includes commercial cameras with dedicated filters used as luminance measuring device and raw spectrometer and present the elaboration of georeferenced images after reconstruction of the unit's inertial pointing along flight trajectory using combined GPS and IMU data integration.**

***Index Terms*—Artificial light at night (ALAN), autonomous payload for sounding balloon, illumination monitoring, trajectory and pointing reconstruction.**

I. Introduction

ARTIFICIAL light at night (ALAN) impacts not only astronomical observations but also alters the biorhythms of the living environment; negative effects linked to excessive illumination have in fact been demonstrated to affect human health [1] and behavior of wildlife [2]. Nighttime light emission is presently monitored using data from orbiting satellites (mainly from visible infrared imaging radiometer suite (VIIRS) aboard SUOMI NPP and NOAA-20 sun synchronous satellites), but satellite's coverage of interest areas is not continuous in time and affected by limited spatial resolution (around 750 m/pixel) [3]. Furthermore, VIIRS operates using a day/night panchromatic band with wavelength range between 500 nm and 900 nm [3] so most radiation from blue LEDs (with energy peak around 450 nm) cannot be detected; these emissions are particularly harmful to star visibility and human health, as underlined by recent reports by International dark Sky Association [4] and American Medical Association [5].

Ground based sky brightness measurements are also locally available, mainly conducted using sky quality meter (SQM) commercial units [6], which are essentially radiometers measuring in the visible bandwidth (within a wavelength range between 400 and 580 nm). SQMs usually provide measures of the zenith brightness of the sky, a quantity affected by artificial light sources spread over a wide area reaching up to hundreds of kilometers from the measuring site ([7] and [8]). Therefore, SQMs quantify the global effect of ALAN looking at a specific portion of the sky. Since usually sky brightness is recorded all night long with time resolution of few minutes, they can used to monitor effects of dimming of outdoor lighting, typically after midnight or to quantify the effect of actions aimed at reducing light pollution. SQMs are often grouped in a network, examples are presented in [9] and [10], thus allowing reconstruction of local maps of the status of the sky. More information on light emission spectral distribution can be obtained by using digital color cameras, either a DSLR camera [11] or the common camera for smartphones [12]. They can provide measures of the overall spatial distribution of the sky brightness, not limited to zenith like SQMs; and elaboration of information from sky color can also be obtained. The information available by terrestrial surveys with either SQMs or color cameras and the data from observations obtained by satellite images need to be merged using dedicated measurement systems able to validate and correlate data on ground radiance and sky brightness; this can be fulfilled using aerial observations at different altitudes and locations using planes or with less expense flying dedicated payloads with drones or balloons. A low-cost autonomous system using commercial cameras with different pass-band filters can in fact efficiently monitor main light emission sources on ground with a resolution of few meter and calibrated photodiodes with ad hoc filters can be used to investigate in parallel sky brightness evolution. Furthermore, by properly controlling the

Manuscript received 19 July 2022; revised 9 February 2023; accepted 10 February 2023. Date of publication 15 February 2023; date of current version 2 March 2023. This work was supported in part by the Department of Industrial Engineering, University of Padova under TWINNING 2017 Grant. *(Corresponding author: Carlo Bettanini.)*

Carlo Bettanini and Pietro Fiorentin are with the Department of Industrial Engineering, University of Padova, 35122 Padova, Italy (e-mail: carlo.bettanini@unipd.it; pietro.fiornetin@unipd.it).

Mirco Bartolomei and Alessio Aboudan are with the Center for Studies and Activities for Space "Giuseppe Colombo", University of Padova, 35122 Padova, Italy (e-mail: mirco.bartolomei@unipd.it2; alessio.aboudan@unipd.it).

Stefano Cavazzani is with the Department of Mechanical and Industrial Engineering, NTNU, 7034 Trondheim, Norway, and also with Department of Physics and Astronomy, University of Padua, 35122 Padova, Italy (e-mail: stefano.cavazzani@unipd.it).

Digital Object Identifier 10.1109/JSTARS.2023.3245190

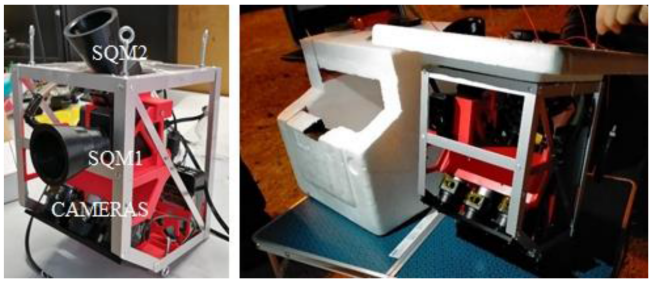

Fig. 1. MINLU autonomous payload architecture for sounding balloon flight.

flight trajectory over a limited area with drones or using tethered balloons it may be possible to track the time evolution of the luminosity over many hours during the night, following the dimming of outdoor and street lights.

II. MINLU Autonomous Payload

"Misurazione dell' INquinamento LUminoso" (MINLU) is a completely autonomous payload system designed to measure sky brightness and in parallel identify and quantify sources of light pollution on ground. It is based on commercial off the shelf components for whole architecture including images acquisition, georeferentiation and storage and thanks to a modular design can be adapted to be used on drones, stratospheric balloons and tethered balloons.

The payload is controlled by a Raspberry PI single-board computer, which performs data acquisition, compression and storage and is connected though a digital hub to the imaging subsystem, which in the baseline flight configuration includes three Basler ace AC A3800-10 digital cameras (two monochromatic and one color) and the sky brightness subsystem, composed by two commercial SQM-LE units. In the imaging subsystem the color camera is used to acquire a global map of the area, one monochromatic camera is provided with a photopic filter and operates as an imaging luminance measuring device (ILMD) and the last monochromatic camera implements a visible transmission diffracting grid with 300 groves/mm to act as a raw multispectrometer.

A commercial Pixhawk Pixcube unit, comprising two IMUs and a GPS module, provides data for trajectory and pointing reconstruction, and operates as transmitting station for the long-range telemetry. Different flight configurations con be easily adopted for drones or balloon; the one for the stratospheric flight includes a power unit providing stable power conversion to all subsystems for at least 5 h of continuous operation reaching an overall mass less than 3 kg comprising thermal insulating cover and flight chain harness. Fig. 1 presents images of the architecture flown in the night flight of July 8, 2020.

III. MINLU Imaging Unit Laboratory Test Campaign

A dedicated test campaign of the image subsystem was conducted at Photometry and Lighting Engineering Laboratory of University of Padova for all cameras and first results have been

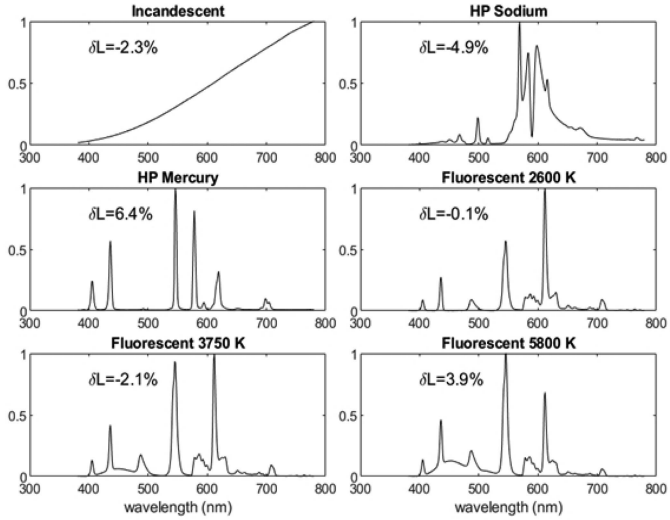

Fig. 2. Comparison between the ILMD and the spot luminance meter Konica Minolta LS-100 in terms of relative error on the measured luminance δL, for different light sources.

Fig. 3. Image of test set up for luminance meter of imaging subsystem (left) alongside reference spot luminance meter Minolta LS-100 and the integrating sphere used for calculation of different CMOS sensor's areas sensitivity (right).

present in [11]; an extended test campaign was afterward conducted focusing on the evaluation of accuracy of performance for luminance meter and raw multispectrometer.

A. MINLU Luminance Meter Calibration

The performance of the MINLU ILMD, composed by a Basler monochromatic camera, Theia lens (model ML410M) and the omega optical photopic filter, has been investigated considering inputs from different types of light sources embracing most commonly used technologies: incandescent lamp, high-pressure sodium lamp, high-pressure mercury lamp and fluorescent low-pressure mercury lamps with different color temperature.

The response of the system has been evaluated considering a spot luminance meter Konica Minolta LS-100 as reference for the direct measurements of the luminance, and a spectroradiometer Konica Minolta CS-1000, to analyze the system sensitivity in the visible wavelength ranges. The detailed description of test set up, shown also in Fig. 3, is reported in [11], although the results of calibration are summarized in Fig. 2 showing a comparison of the output of MINLU ILMD with the reference spot luminance meter: the relative error on the measured luminance δL is reported on top of the measured spectra of the input light.

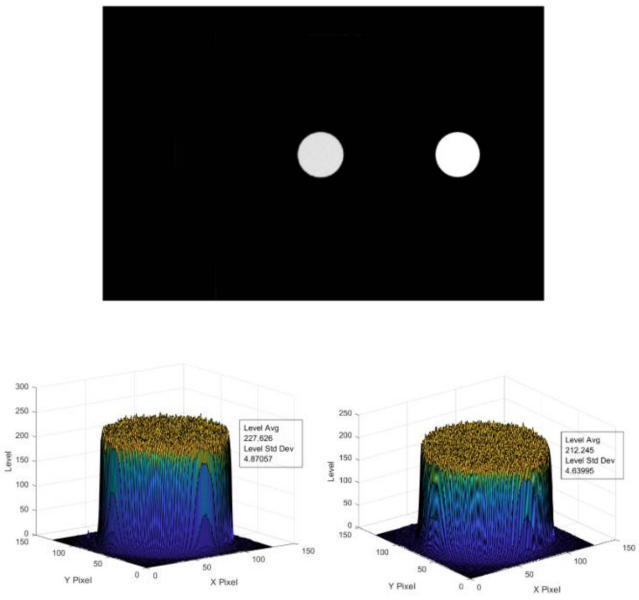

Fig. 4. Input luminance areas and elaboration of average pixel level at central (bottom left) and side (bottom right) CMOS sensor location for the highest input luminance (around 2.64 cd/m^2).

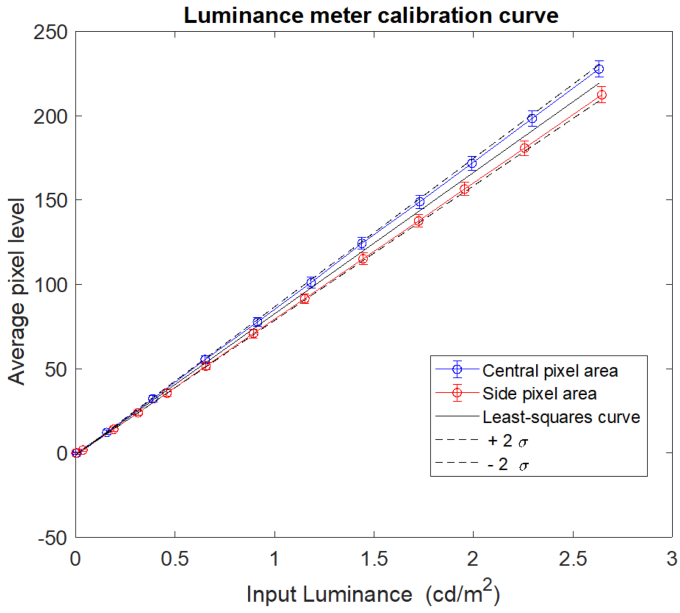

Fig. 5. Least-squares luminance meter calibration curve obtained with the elaboration of images of central and side areas of CMOS sensor.

The highest error versus the reading of the reference luminance meter is below 7% (related to the HP mercury source characterized by sharp peaks in the spectrum) therefore the realized low cost MINLU luminance meter can be considered a useful instrument for the analysis of polluting light sources.

Furthermore, to accurately reconstruct luminance from ground sources in the whole field of view of the camera, the luminance meter's sensitivity in different areas of the complementary metal oxide semiconductor (CMOS) sensor matrix and with different directions of the incoming light has been investigated by varying the relative position and input value from an integrating sphere with diameter of 38 mm; luminance input has been in parallel measured with a reference spot luminance meter Konica Minolta LS-100.

The conducted analysis was aimed at checking the system linearity, the response uniformity and at evaluating the vignetting in camera's sensor.

Fig. 4 reports the elaboration of data for the highest input luminance provided by the integrating sphere (input luminance around 2.64 cd/m^2), showing the acquired images and the reconstruction of average pixel values and standard deviation for central and lateral CMOS areas. For both cases, centered and the side, the local uniformity of the levels detected by the CMOS sensor was within 1%.

The analysis of data for the central and side areas of the pixel matrix allowed to elaborate a least-square curve representing the average response of ILMD pixel to an input luminance coming by any position in the field of view and provides an evaluation of vignetting of the ILMD's sensor. The least square curve including uncertainty bands is reported in Fig. 5 along with the specific curves for central and side areas: the two sigma (95% confidence) uncertainty band assigned to ILMD pixel sensitivity is below 2% of average sensitivity value.

The overall accuracy of the ILMD sensor can be therefore evaluated assigned the combined uncertainty considering contributions from the worst-case error in the response to different types of light sources (ur) which is considered as a three-sigma interval ($k = 3$ or 99.8% confidence) and the above presented uncertainty related to vignetting (uv) a two-sigma interval ($k = 2$ or 95.4% confidence).

The uncertainty contributions can be considered uncorrelated and therefore the ILMD overall uncertainty can be written as in

$$u_{\text{ILMD}} = \sqrt{\left(\frac{u_r}{3}\right)^2 + \left(\frac{u_v}{2}\right)^2} \tag{1}$$

where considered values for *ur* and *uv* are, respectively, 6.4% and 2% of measured luminance (L). The relative uncertainty for ILDM measurement can therefore be evaluated as

$$u_{p\ \text{ILMD}} = \frac{u_{\text{ILMD}}}{L} \approx 2.35\% \tag{2}$$

or

$$u_{p\ \text{ILMD}} = \frac{u_{\text{ILMD}}}{L} \approx 4.7\% \tag{3}$$

using a 95% confidence interval ($k = 2$).

B. MINLU Raw Multispectrometer Calibration

The wavelength calibration of the MINLU raw multispectrometer has been obtained using the input from different light sources and comparing the output with a reference CS-1000 Konica Minolta portable spectroradiometer. Fig. 6 reports the results of the comparison using inputs from an high-pressure sodium lamp, a high-pressure mercury lamp, a PC Amber LED and three fluorescent low-pressure mercury lamps with different color temperature. To allow a direct comparison of the output of the two spectrometers, the areas under the shown spectra are normalized, so both instruments receive the same total power

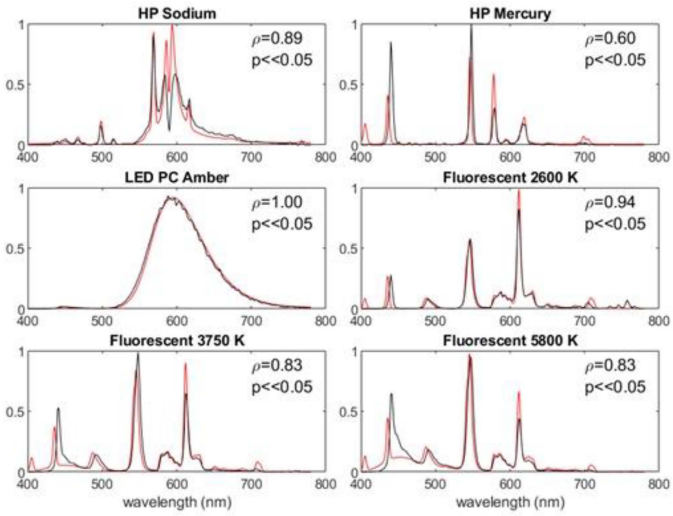

Fig. 6. Comparison between spectra measured by the multispectrometer (black line) and the reference spectrometer Konica Minolta CS-1000 (red line) used to quality of the spectra reconstruction by the multispectrometer.

coming from the observed source. The similarity of the spectra measured by the two instruments was quantified in [11], while Fig. 6 reports the result obtained for newly elaborated spectra correlation along with the probability of the null hypothesis, which was less than 5% for all the tests.

In the case of input from the PC Amber LED (characterized by a broadband spectrum with smooth shapes), the achieved correlation is close to 1 while the multispectrometer shows lower accuracy when reconstructing input signals with sharp peaks (sodium and mercury lamps), as it is highlighted by the reduced values of the correlation and the spread of the power around the peaks.

For the mercury lamp (high-pressure and low-pressure), the difference between the two spectral measurements is evident looking at the peak at 436 nm (red line from CS-1000), which is shifted at 440 nm by the multispectrometer. Furthermore, an even stronger discrepancy is present for wavelengths below 420 nm, caused by the strong attenuation of the lens used in the multispectrometer and the reduced sensitivity of the Basler camera. Although this frequency range is not crucial for the analysis of the ALAN, the problem can be in any case mitigated by using ultraviolet lenses.

Considering that the aim of MINLU raw multispectrometer is the identification of light source technology, the results of calibration show that the system can be effectively used during the flight to correlate the reconstructed spectrum with the type of illumination.

IV. MINLU Flight Data Elaboration

The MINLU flight operation was the result of a collaboration between the Department of Industrial Engineering and the Center of Studies and Activities for Space "G. Colombo" of University of Padova which designed and tested the balloon's gondola flight hardware; Space Systems Lab from University

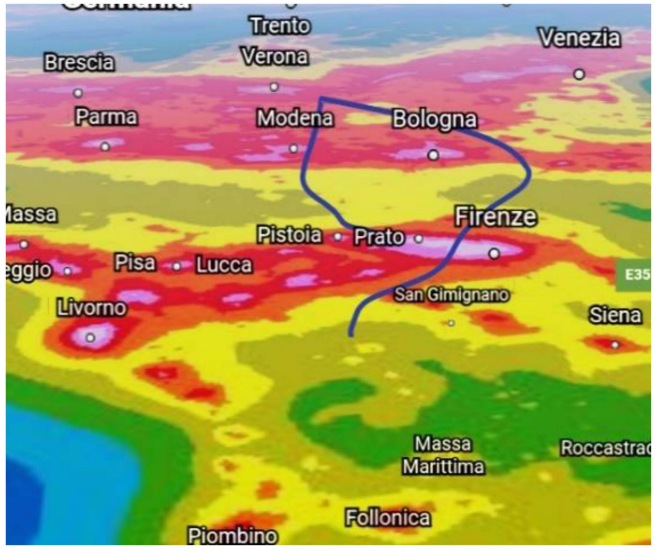

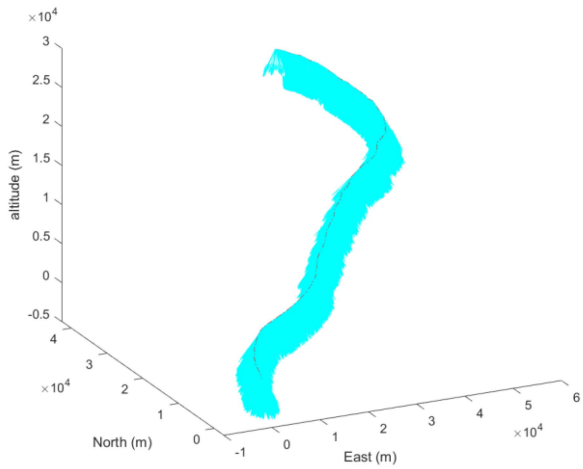

Fig. 7. Reconstructed flight trajectory over light pollution map based on VIIRS data (top) and reconstructed pointing in NED reference centered at launch site (bottom).

of Pisa provided its UniPiHAB04 flight train to safely perform launch and recover activities.

MINLU payload was successfully launched around 1.15 AM on July 8 2021 during astronomical night condition; the total flight time was 3 h and 15 min with a maximum achieved altitude around 34 km. The imaging unit operation was started 30 min before launch and logging ended later than 5 hours after total stored battery energy was consumed; color camera, luminance meter and raw multispectrometer were acquired at a 12 s interval, resulting in 8 GB of saved data (approximately 2900 raw images) for the whole flight.

The flight trajectory has been reconstructed from GPS data and transformed in a NED inertial reference centered at launch site (Lajatico) to calculate pointing direction of the imaging unit and allow image georeferencing. The reconstructed flight trajectory is reported in Fig. 7 along with the calculated absolute pointing during ascent to stratospheric altitude.

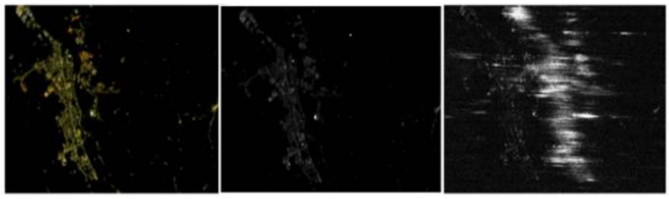

Fig. 8. Image of Certaldo area from color camera (left), ILMD (center) and raw multispectrometer camera (right), this last adjusted in intensity for view.

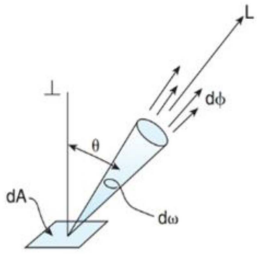

$$L = \frac{dI}{dA\cos\theta}$$

$$where\ dI = \frac{d\Phi}{d\omega}$$

Fig. 9. Representation of calculation of Luminance (L) detected at angle θ from vertical.

The payload attitude and consequently the inertial pointing direction of the imaging system has been calculated elaborating measures of inertial sensors (IMU magnetometers, rate gyros and accelerometers) with a dedicated Kalman filter. Once inertial pointing has been reconstructed the acquired images have been georeferenced using the combined information from trajectory and attitude. As an example, Fig. 8 reports the images acquired by MINLU when floating over the area of Certaldo, a medium size town in Tuscany, at an altitude of 8494 m; reconstructed attitude of the payload shows a limited tilting (pitch 2.3°, roll −1.2°, yaw −185.6°).

A. MINLU ILMD Data Elaboration

Luminance L can be calculated as the quotient of luminous intensity dI in a given direction produced by an element of surface dA, by the area of the orthogonal projection of the element on a plane perpendicular to the given direction (θ). The mathematical relation is presented below in Fig. 9 where $d\Phi$ is the luminous flux related with the spherical angle $d\omega$.

The correct estimation of illumination from ground areas is therefore possible only after elaborating the trajectory and attitude of the balloon's payload; this allows the calculation of angle θ and area dA, depending on current altitude and total tilt of the MINLU payload. In this article, dA is considered as the area on ground imaged by a single pixel of the CMOS matrix of sensor of ILMD and θ the relative view angle derived by payload attitude; dI will therefore estimate the average illumination from the area dA as

$$dI = L\, dA \cos\theta. \tag{4}$$

Considering that the imaging system of MINLU payload was installed at a 35° angle in respect to nadir direction (see Fig. 10), ground sample distance varies along the CMOS matrix showing lower values for the CMOS line aligned with the direction closer to the nadir. With a zero angle of vertical tilt the developed

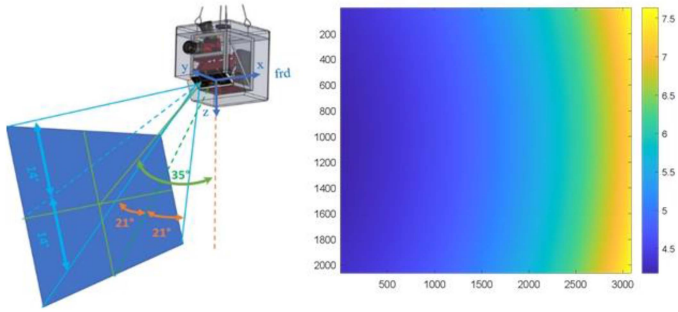

Fig. 10. Sketch of area within the field of view of imaging subsystem (left) and projected surface area (in m^2) related to pixel of CMOS matrix (right).

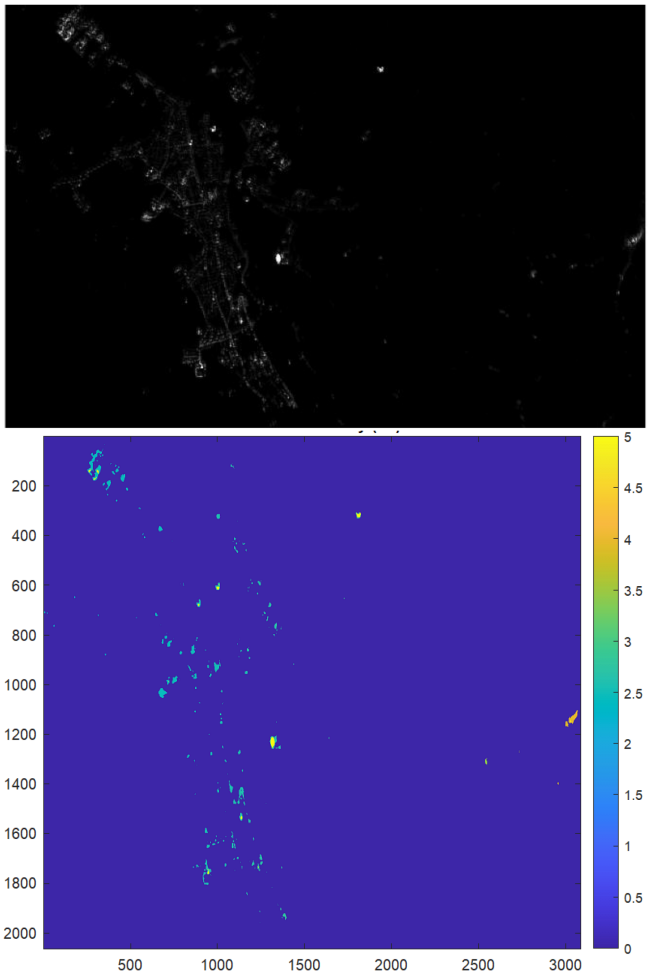

Fig. 11. Image of the Certaldo area from ILMD at 8494 m altitude (top) and reconstructed luminous intensity (in cd) of the surrounding area (bottom).

luminance meter can achieve a ground sample distance of 3 centimeter when at 200 m altitude, increasing the value to 8 m at 34 km; this last still considerably improving the ground resolution of satellite data [VIIRS panchromatic day/night band (DNB) data resolution is 750 m].

A sketch of the area monitored within the field of view of imaging subsystem is provided in Fig. 10 where the characteristic angles of FOV aperture depending on CMOS geometry (3088 x 2064) are also presented (±21° and ±14°). The plot in

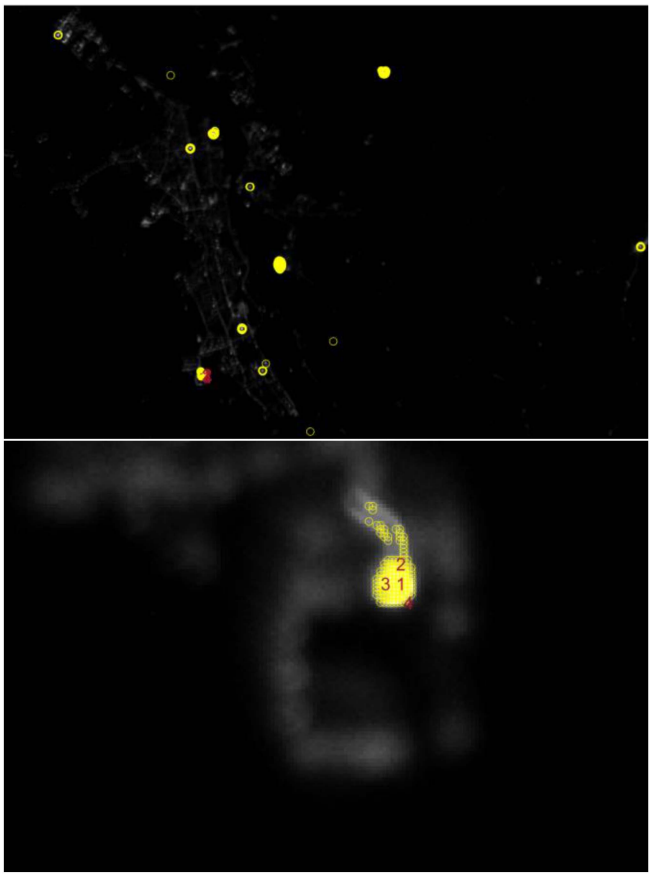

Fig. 12. Identification of emission areas above 5 cd illumination (top) and zoomed image of the area of interest in the lower left part of image.

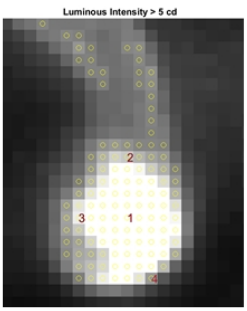

Pixel	Pixel Area on ground (m^2)	Calculated Illumination (cd)	Uncertainty (cd)
1	4.631	7.70	0.36
2	4.630	5.13	0.25
3	4.628	7.69	0.37
4	4.633	5.12	0.26

Fig. 13. Identification of some areas of emission and results of calculation of illumination for Certaldo overpass.

the right part of same figure reports the calculated areas for every pixel during the passage over Certaldo at 8494 m altitude (with a reconstructed inertial attitude for MINLU probe as follows: pitch 2.3°, roll −1.2°, yaw −185.6°).

The characterization of light emission is then achieved using calibration data for pixel sensitivity and performing conversion of pixel values in upwards average luminous intensity in candles using (4). An image acquired by ILMD over the Certaldo area at 8494 m altitude is shown in Fig. 11 along with the elaborated values for luminous intensity from ground areas. Fig. 12 presents the identification of illuminating areas with reconstructed illumination values higher than five candles.

Fig. 14. Color image of Pistoia area near from 34 km altitude.

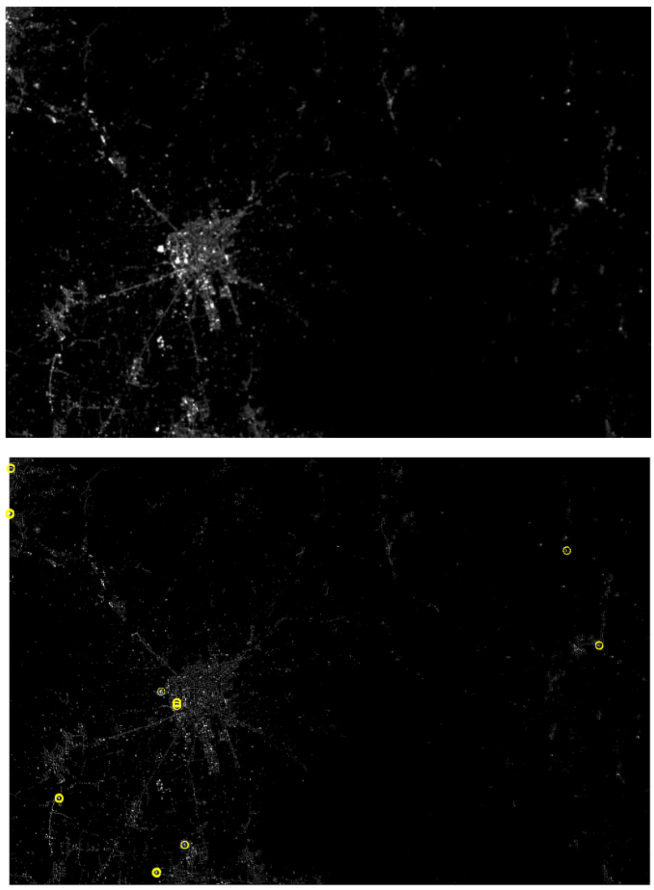

Fig. 15. Luminance camera image of the Pistoia area from 34 km altitude (top), areas with reconstructed average luminous intensity above 100 cd (bottom).

The uncertainty in the estimation of illumination values can be calculated referring to (4) and considering that uncertainty in Luminance L is the uncertainty of ILMD evaluated in (3) and uncertainties of angle θ and area dA can be calculated depending on uncertainty of attitude (u_{att}) and altitude (u_{alt}) reconstruction. The uncertainty of probe attitude can be evaluated in 1.0° for each Euler angle by combining attitude sensor uncertainty and average noise on reading due to flight induced

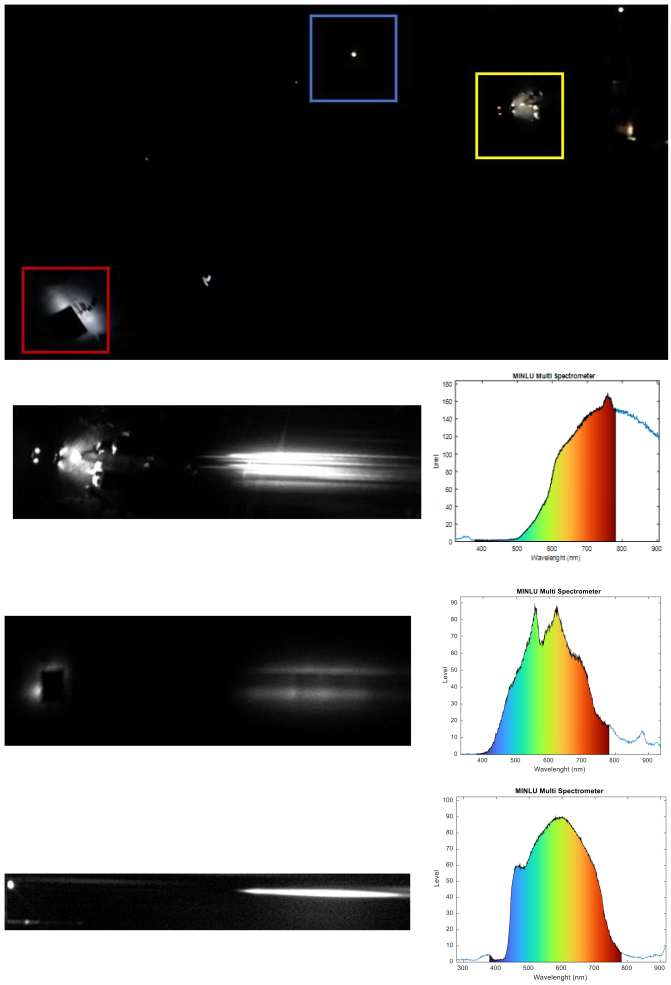

Fig. 16. Image of launch site taken from color camera (top) showing car illuminating the launch pad (yellow rectangle), one garden lamp (blue rectangle) and nearby illuminated house (red rectangle) and respective elaboration of emitted light spectrum from multispectrometer.

oscillations. Pointing error uncertainty can therefore evaluated as $u_{\mathrm{att}} = 1.75°$.

Uncertainty on altitude reconstructed from GPS data is in the order few meters over several kilometer altitude; so, because of the low relative value, can be disregarded in calculation. The uncertainty of the value for pixel area *dA* can be evaluated considering as worst-case value the biggest area of the CMOS uncertainty matrix; the uncertainty is a function of altitude and attitude and can be considered to be within 6% of the calculated area considering a uniform interval with 100% confidence.

By considering *dI* in (4) as a function of L, *dA* and θ and by renaming such variables as $x1$, $x2$, and $x3$ (5) can be used for combined uncertainty calculation

$$u_{dI} = \sqrt{\left(\frac{\partial f}{\partial x_1}\right)^2 u_{x_1}^2 + \left(\frac{\partial f}{\partial x_2}\right)^2 u_{x_2}^2 + \left(\frac{\partial f}{\partial x_3}\right)^2 u_{x_3}^2} \tag{5}$$

where $x1 = u_{\mathrm{ILDM}} = 2.35\%$ of reading, $x2 = u_{\mathrm{dA}} = 6\%$ of calculated area / $\sqrt{3}$, $x3 = u_{\mathrm{att}} = 1.75°$.

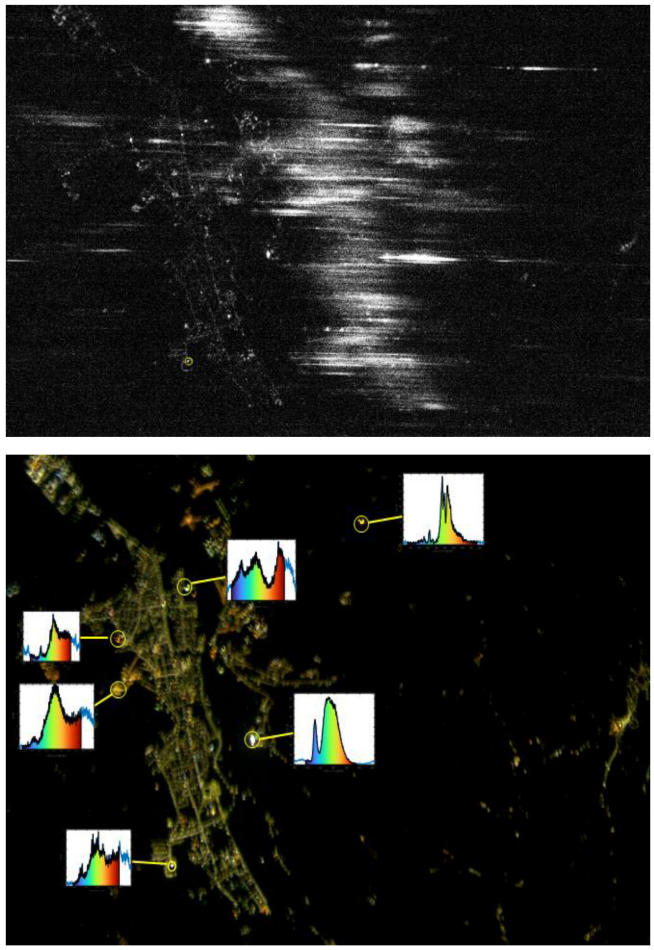

Fig. 17. Image of Certaldo area from raw multispectrometer camera (top), and reconstructed spectra of main sources shown over the color camera image (bottom).

The developed algorithm for illumination evaluation calculates in parallel illumination levels and related uncertainty. Results for the Certaldo area are reported in the following Fig. 13, where presented uncertainty is scaled to one sigma interval (68% confidence).

The same procedure has been utilized for the evaluation of illumination by ground sources up to burst altitude of 34 km; as altitude is increasing projected surface area for the pixels of ILMD's CMOS matrix increases accordingly, lowering resolution of lowest detectable luminous intensity. Fig. 14 reports one image by color camera of the Pistoia area at 34 km altitude; the calculated projected surface area of pixels of the CMOS matrix ranges from 65 to 125 m. The image from luminance meter camera and its elaboration identifying ground areas with values of the average luminous intensity above the threshold of 100 cd are presented in Fig. 15.

B. MINLU Raw Multispectrometer Flight Data Elaboration

Fig. 16 presents an image of launch site taken few seconds after take-off from the color camera and the elaboration of the relative multispectrometer image showing the obtained spectra from lights associated with the car illuminating the area of the

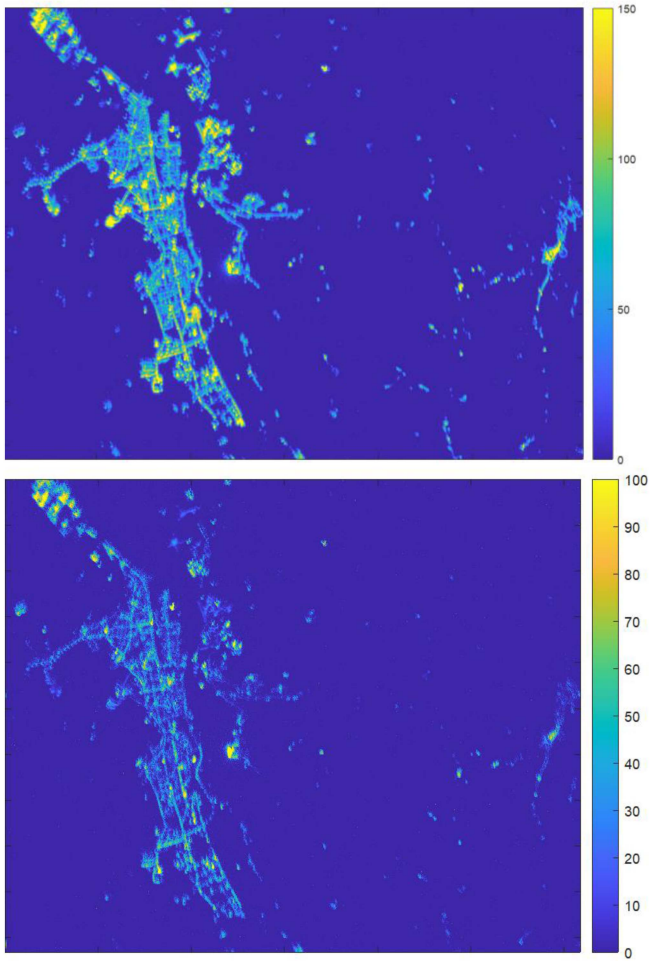

Fig. 18. Red level of RGB image from color camera (top), blue level of RGB image from color camera (bottom).

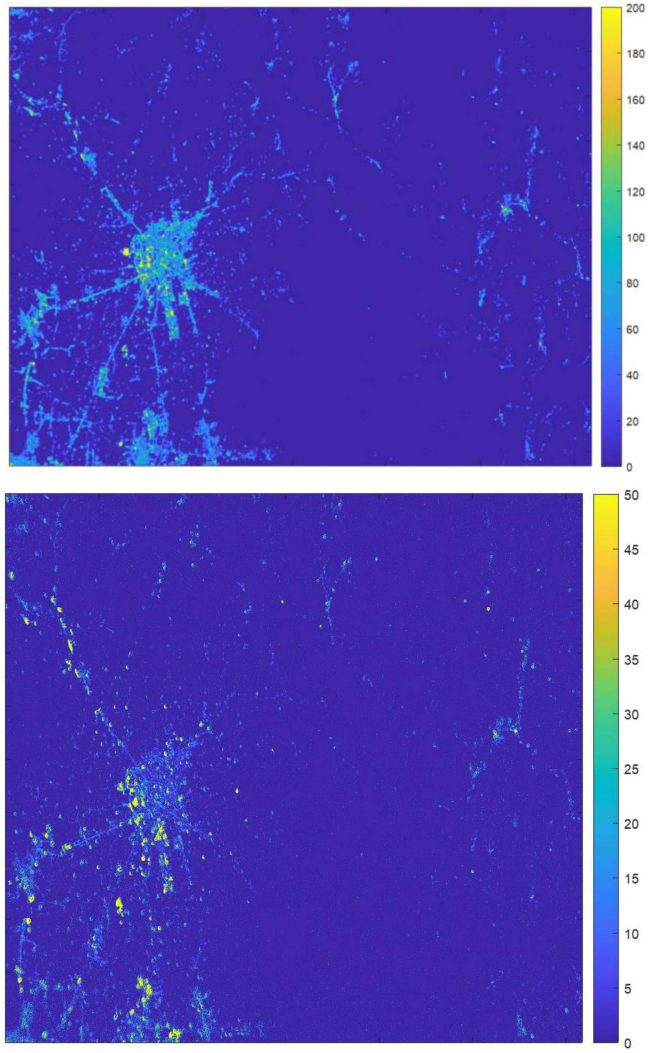

Fig. 19. Image of Pistoia area with levels in red RGB band (top) and blue RGB band (bottom).

launch pad, one garden lamp and a nearby house. It is evident that the spectrometer images allow to discriminate among the different illumination technologies used in the ground sources.

The number of light sources present in the spectrometer field of view and consequently the number of spectral lines generated in the image increases with altitude thus decreasing the capability to investigate single sources, but producing an average spectrum of an interest area.

Fig. 17 on the left reports the image acquired by the raw spectrometer when floating over Certaldo at an altitude of 8494 m. Although the number of diffraction lines is quite high, it still possible to reconstruct emission spectrum of main areas of interest which are shown over the color camera image.

Right part of Fig. 17 presents the calculated spectra of main light polluting zones; it is still possible to calculate an average spectrum but the accurate guess of the illumination technology is possible only for areas with sites of uniform illumination (parking, industrial sites …). Information on the prominent emission in the blue or red area can also be extracted from the RGB levels of the color camera image, achieving coherent information with the one elaborated using spectrometer data (see Fig. 18).

At higher altitudes spectra from the multispectrometer tend to overlap reducing the accuracy of light-type reconstruction so only a qualitative analysis of type of illumination is possible by considering the image from color camera and the levels in the red or blue color region. Fig. 19 reports the elaboration of color image of Pistoia area from 34 km altitude highlighting the areas emitting in red and blue RGB band.

V. Conclusion

An autonomous scientific payload for monitoring ground sources of light pollution has been developed at University of Padova and tested in a sounding balloon night flight on July 8, 2021. Based on commercial components and with extremely limited mass and dimensions the systems has been able to guarantee continuous operation for more than 5 h providing data on ground generated ALAN up to 34 km altitude.

Flight data have been used to analyze ground emission, quantifying levels of illumination and power spectral distribution linking them to sources of artificial luminance; data from raw

multispectrometer have been successfully used at low altitude to accurately identify ground source's illuminating technology; at higher attitudes mainly levels in RGB bands are used to have a qualitative insight of "warm" or "cold" emission sources. Levels of upward emitted light from areas of interest have been evaluated from images of luminance meter camera based on laboratory calibration and correct reconstruction of inertial attitude of the payload.

The limited dimensions and mass of the unit (3 kg) along with the modularity of its architecture allow to use the developed system on drones and tethered balloons and significantly overcomes the performance achievable by satellites images in discriminating among the different light sources used for street and outdoor lighting.

References

[1] J. Shen and J. Tower, "Effects of light on aging and longevity," *Ageing Res. Rev.*, vol. 53, 2019, Art. no. 100913.

[2] L. L. Bliss-Ketchum, C. E. de Rivera, B. C. Turner, and D. M. Weisbaum, "The effect of artificial light on wildlife use of a passage structure," *Biol. Conserv.*, vol. 199, pp. 25–28, 2016.

[3] L. B. Liao, S. Weiss, S. Mills, and B. Hauss, "Suomi NPP VIIRS day-night band on-orbit performance," *J. Geophys. Res., Atmos.*, vol. 118, pp. 12,705–12,718, 2013, doi: 10.1002/2013JD020475.

[4] International Dark-Sky Association white paper, "Visibility, environmental, and astronomical issues associated with blue-rich white outdoor lighting," May 4, 2010. [Online]. Available: https://www.darksky.org/wp-content/uploads/bsk-pdf-manager/8_IDA-BLUE-RICH-LIGHT-WHITE-PAPER.PDF

[5] American Medical Association report, "Human and environmental effects of light emitting diode community lighting," CSAPH Tech. Rep. 2-A-16, 2016. [Online]. Available: https://policysearch.ama-assn.org/councilreports/downloadreport?uri=/councilreports/a16_csaph2.pdf

[6] "Globe at night - Sky brightness monitoring network (GaN-MN)," Accessed: Feb. 11, 2023. [Online]. Available: https://www.globeatnight.org/gan-mn.php

[7] A. Jechow et al., "Tracking the dynamics of skyglow with differential photometry using a digital camera with fisheye lens," *J. Quant. Spectrosc. Radiative Transfer*, vol. 209, pp. 212–223, 2018.

[8] P. Fiorentin et al., "Calibration of digital compact cameras for sky quality measures," *J. Quant. Spectrosc. Radiative Transfer*, vol. 255, 2020, Art. no. 107235.

[9] A. Bertolo et al., "Measurements of night sky brightness in the Veneto region of Italy: Sky quality meter network results and differential photometry by digital single lens reflex," *J. Imag.*, vol. 5, no. 5, 2019, Art. no. 56.

[10] S. Bará, R. C. Lima, and J. Zamorano, "Monitoring long-term trends in the anthropogenic night sky brightness," *Sustainability*, vol. 11, no. 11, 2019, Art. no. 3070.

[11] P. Fiorentin, C. Bettanini, and D. Bogoni, "Calibration of an autonomous instrument for monitoring light pollution from drones," *Sensors*, vol. 19, 2019, Art. no. 5091.

[12] S. Tominaga, S. Nishi, and R. Ohtera, "Measurement and estimation of spectral sensitivity functions for mobile phone cameras," *Sensors*, vol. 21, 2021, Art. no. 4985.

Carlo Bettanini received the B.Sc. degree in mechanical engineering and the Ph.D. degree in "space science and technology" from the University of Padova, Padova, Italy, in 1997 and 2002, respectively.

He is currently an Assistant Professor of "Aerospace Flight Dynamics" with the Department of Industrial Engineering, University of Padova and has led several research projects dedicated to the development of new instruments to monitor environmental parameters in low, medium and high Atmosphere.

Mirco Bartolomei received the B.Sc. degree in mechanical engineering from the University of Padova, Padova, Italy, in 2015.

He is a Young Researcher with the Center for Studies and Activities for Space "Giuseppe Colombo," University of Padova collaborating on thermo mechanical design and AIT of space instruments.

Pietro Fiorentin received the B.Sc. degree in electronic engineering and the Ph.D. degree in electrical engineering from the University of Padova, Padova, Italy, in 1988 and 1991, respectively.

He is a Professor of "electrical measurements" and "light engineering and photometry" with the University of Padova, Padova, Italy. His researches concern with photometry and radiometry, with care to the effect of the outdoor artificial lighting called "light pollution." He is a Coordinator of Italian Division 2 "Physical Measurement of Light and Radiation" of the Commission Internationale de l'Éclairage.

Alessio Aboudan received the B.Sc. degree in software engineering and the Ph.D. degree in "mechanical measurements" from the University of Padova, Padova, Italy, in 2001 and 2006, respectively.

He is currently a Researcher with the Center for Studies and Activities for Space "Giuseppe Colombo," University of Padova with more than 20 years of experience in scientific sensors design, software development and data analysis techniques for space applications.

Stefano Cavazzani received the B.Sc. and Ph.D. degrees in astronomy from the University of Padova, Padova, Italy, in 2006 and 2014, respectively.

He is a Researcher with the Department of Mechanical and Industrial Engineering, NTNU, Trondheim, Norway and with the Department of Physics and Astronomy of the University of Padua; he collaborates with INAF as an expert of atmospheric quantum transmission, big data analytics, and development and calibration of instruments and sensors for atmosphere characterization.